XI International Conference on Computational Plasticity. Fundamentals and Applications
COMPLAS XI
E. Oñate and D.R.J. Owen (Eds)

NON-LINEAR FINITE ELEMENT ASSESSMENT ANALYSIS OF A MODERN HERITAGE STRUCTURE

STEFANO SORACE[*] AND GLORIA TERENZI[†]

[*] Department of Civil Engineering and Architecture
University of Udine
Via delle Scienze 208, 33100 Udine, Italy
e-mail: stefano.sorace@uniud.it

[†] Department of Civil and Environmental Engineering
University of Florence
Via di S. Marta 3, 50139 Florence, Italy
e-mail: terenzi@dicea.unifi.it

Key words: Non-linear Finite Elements, Structural Assessment, Steel, Reinforced Concrete, Buckling, Smeared Cracking.

Abstract. A synthesis of a non-linear finite element structural assessment enquiry carried out on a monumental modern heritage building is reported in this paper. The study includes a buckling analysis of the slender steel beams constituting a mushroom-type roof, and an "integral" seismic pushover analysis of the supporting R/C columns. The computational solutions obtained for the steel roof beams are compared to the results derived from a calculation of the critical stress of beam panels, and the global lateral-torsional buckling resistance of members developed according to the Technical Standards adopted for structural verifications. The unconventional "full-cracking" pushover application to the R/C columns offers detailed simulation of the evolution of their non-linear response, which is discussed in the paper, along with the most significant parameter and procedure choices made in the analysis.

1 INTRODUCTION

Non-linear finite element approaches are suggested in the latest generation of international Technical Standards as preferential analysis methods for the static and seismic assessment of existing structures. This prompts an extension of the use of non-linear models and calculus programs, which are typically conceived, developed and implemented in the academic community for research aims, to the professional community of structural engineers. An important role can be played by academicians also at this challenging phase, where a critical review of the theoretical options and of the limits of available models, as well as an expert guidance to their practical application, are urged by professional users.

A study in this field is currently being carried out by the authors within a National Research Project, financed by the Italian Ministry of Education and University and dedicated to the historical and structural analysis of Italian modern heritage architecture built in the

1950s and in the 1960s. Special care is devoted in this paper to a representative masterpiece building, the "Palazzo del Lavoro" in Turin, designed in 1959 by the world-famous Italian engineer Pier Luigi Nervi, and completed in 1961. The main structural elements of the building consist of sixteen monumental reinforced concrete (R/C) columns, 20 m high, and sixteen supported steel mushroom roof panels, each covering an area of 40×40 m×m. The building includes other monumental structural members, and namely the R/C ribbed slabs typical of Nervi's style, which constitute the two perimeter gallery floors, and the continuous gallery-to-roof glass façades. External views of the building at the time of its opening and in its current conditions; the plans of the roof and upper gallery floors; the elevation design drawing and a view of a mushroom steel roof panel and relevant R/C column, are shown in Figures 1, 2 and 3, respectively.

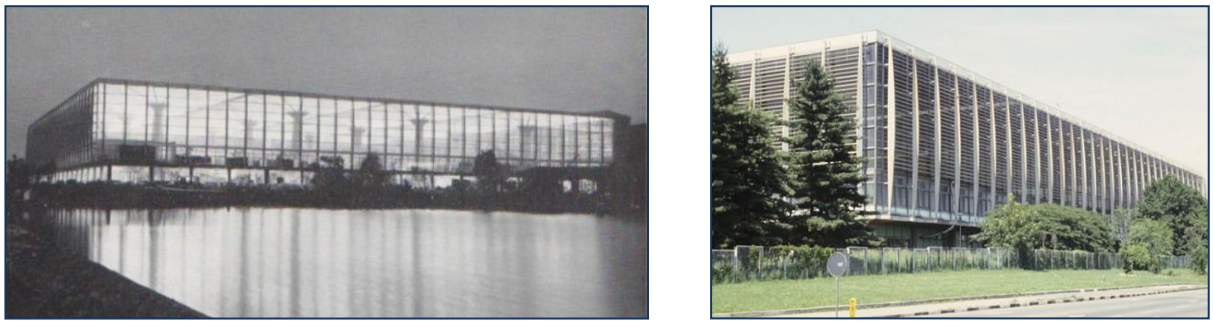

Figure 1: External views of the building at the time of its opening and in its current conditions

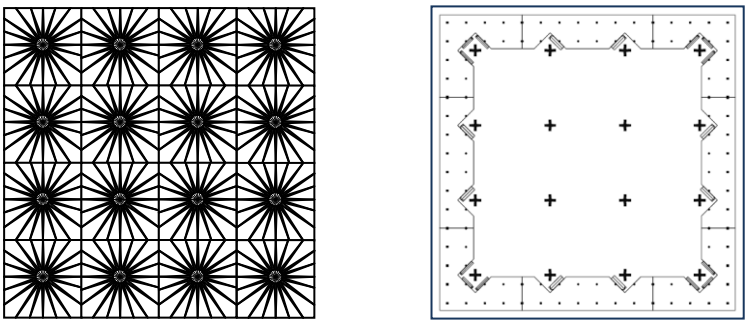

Figure 2: Plans of the roof and the upper gallery

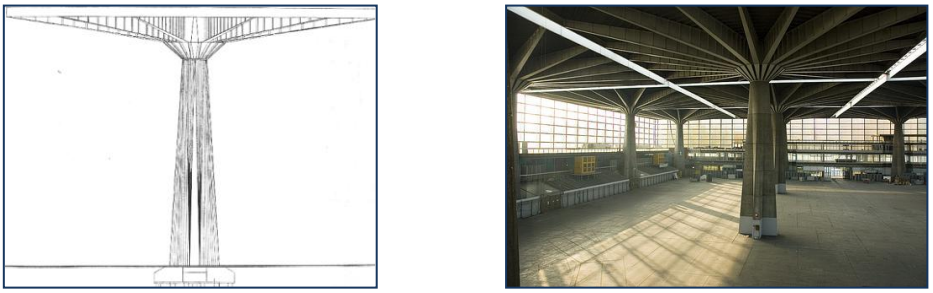

Figure 3: Elevation design drawing and view of a mushroom steel roof panel and the supporting R/C column

Linear elastic finite element analyses of these structural elements taken separately, as well as of the entire building, were initially carried out to evaluate their static and dynamic characteristics, and to check their current nominal safety conditions [1]. Based on the results of this first-level assessment analyses, a second-level step was then undertaken, aimed at carefully evaluating the structural performance of the two most important types of members, i.e., the steel roof beams and the R/C monumental columns. This new section of the numerical study posed two representative problems of non-linear geometrical—steel beams—and material—R/C columns—type, respectively.

A local and global buckling analysis was developed for the roof beams, in order to investigate the instability effects arising from their very slender sections. Similarly to many other finite element commercial codes, the SAP2000NL [2] program used for this analysis produces a not plainly understandable buckling mode calculation, which leaves uncertainties both on the non-linear geometrical formulation of the problem and the final results. These aspects were investigated by comparing the computational solutions with the results derived from the expressions of the critical stress of panels and the global lateral-torsional buckling resistance of beams provided by the reference Technical Standards on steel structures adopted for the structural verifications [3-6].

The R/C columns were evaluated with an "integral" seismic pushover analysis of the numerical model constituted by a full mesh of solid octahedral smeared cracking "concrete" elements with embedded steel reinforcements, generated by the ANSYS non-linear calculus program [7]. No reductions to simplified models were considered in this enquiry, as the "uniform resistance" columns designed by Nervi should ideally reach the first significant cracked configurations, and then the plasticization of vertical reinforcements, simultaneously in several sections along the height. This "full-cracking" application offers a more direct and realistic simulation of the evolution of the non-linear response of columns as compared to models including lumped plastic hinges or fiber-composed plastic zones, but it requires a much greater computational effort, more careful choices of the mechanical and algorithmic parameters, and proper checks on the stability and accuracy of the solution.

A synthesis of the analyses carried out on the roof steel beams and the R/C columns is presented in the following two sections.

2 ANALYSIS OF STEEL ROOF BEAMS

The 20 cantilever steel radial beams forming the corolla of each one of the 16 mushroom panels of the roof have fixed-end bolted connections to a circular drum, constituted by 20 rectangular steel frames, whose height is 2800 mm and whose base is 1900 mm. Each frame is supported by a triangular steel plate—with a 1500 mm-long vertical side and a 1900 mm-long horizontal side—placed over a 200 mm-deep groove on the upper section of the R/C column (Figure 4). The I-section welded beams, which are joined on their free end to a continuous C-shaped steel edge beam outlining the square perimeter of the mushroom panel, are 2800 mm to 700 mm high, and their top and bottom flanges are 690 mm to 200 mm wide. The beams have three different spans, ranging from 15,750 mm (type 1 beams, orthogonal to the C edge profile) to 20,250 mm (type 3 beams, close to the diagonal of the square). The constituting steel is equivalent to the current S235JR type, with yielding and ultimate nominal stress values f_y=235 MPa and f_u=355 MPa, respectively. The web of the beams is very thin (5

mm—type 1 through 7 mm—type 3); this determines a high slenderness of cross sections, especially in the areas close to the fixed end. The web is subdivided in 13 (type 1 beam) through 17 (type 3) panels by a set of vertical stiffening plates welded to the web and to the top and bottom flanges. The different web thickness and stiffener spacing values determine a very similar resistance of the three types of beams to bending and shear stresses, as well as to local and global buckling, as planned in the original design of the metallic roof (carried out by engineer Gino Covre, who worked with Pier Luigi Nervi for this part of the building structure). In view of this, the finite element and verification analyses are synthesized below for type 1 beams, whose dimensions are reported in Figure 4, as they are also representative of the remaining two beam types.

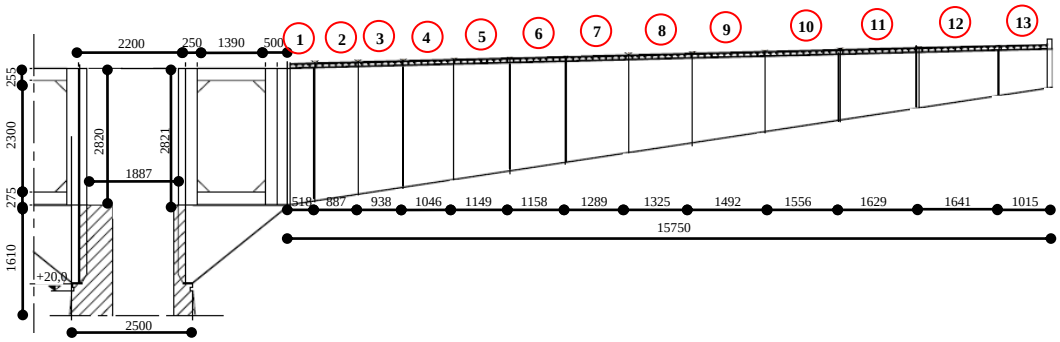

Figure 4: Upper section of a R/C column and relevant steel drum, and view of a triangular bearing plate and a type 1 cantilever beam (dimensions in millimeters)

2.1 Bending and shear resistance and lateral-torsional buckling verifications

The resistance verification to the in-plane bending moment at the ultimate limit states—carried out by referring to the effective properties of Class 4 cross-sections, to which the considered members belong according to Eurocode 3 Part 1-1 rules [3]—is not met. Indeed, the ratio of the design value of bending moment to the corresponding design resistance is significantly greater than 1 (and it reaches 1.57 for the fixed-end section) along over 3/4 of beam span. The resistance verification to shear stress is met for all sections. The verification at the serviceability limit states concerning vertical deflection, developed according to the current Italian Technical Standards [5] (as Eurocode 3 devolves this specification to the National Annexes), is widely met too.

The verification of the beams to lateral-torsional buckling was carried out by considering the only effect of the major axis bending, since the compression axial force induced by the slope of the center-line of the beams is very low (with a maximum of 22 kN at the fixed-end section). The relevant verification formula is:

$$\frac{M_{Ed}}{M_{b,Rd}} < 1 \tag{1}$$

where M_{Ed}, $M_{b,Rd}$ are the design value of the moment and the design buckling resistance moment, respectively, with $M_{b,Rd}$ expressed as:

$$M_{b,Rd} = \chi_{LT} W_y \frac{f_y}{\gamma_{M1}} \tag{2}$$

being $W_y=W_{eff,y}$ for Class 4 sections ($W_{eff,y}$ is computed by determining the effective section as a function of the reduction factor ρ for the compressed portion of the web and the compressed flange), f_y=235 MPa, as noted above, and γ_{M1}=1.05; χ_{LT} is given by the following relation:

$$\chi_{LT} = \frac{1}{\Phi_{LT} + \sqrt{\Phi_{LT}^2 - \bar{\lambda}_{LT}^2}} \tag{3}$$

where $\Phi_{LT} = 0.5\left[1+\alpha_{LT}\left(\bar{\lambda}_{LT}-0.2\right)+\bar{\lambda}_{LT}^2\right]$, α_{LT} is an imperfection factor, equal to 0.76 for welded I-sections with height-to-base ratio greater than 2, $\bar{\lambda}_{LT} = \sqrt{\frac{W_y f_y}{M_{cr}}}$, and M_{cr} is the elastic critical moment for lateral-torsional buckling evaluated according to the expression in Annex F of [3]. By applying the relations above, the ratio of M_{Ed} (equal to 2414 kNm) to $M_{b,Rd}$ (1415 kNm) results to be equal to 1.706, and thus the verification inequality (1) is definitely not met. The unsafety factor is obtained by inverting the ratio between the two moments ($M_{b,Rd}$/ M_{Ed}=1/1.706), i.e. 0.586.

2.2 Web panel buckling verifications

The web panels are much more sensitive to buckling than the flange plates are, as a consequence of the high slenderness of the web determined by the geometrical characteristics of the beams. The verification analysis is carried out in this case by referring to the criterion proposed in a previous edition of the Italian Standards for steel structures [6], where the effects of normal and shear stresses are jointly considered, assuming an ideal critical stress $\sigma_{cr,id}$ to be compared to the design ideal stress computed according to the von Mises rule. The expression of $\sigma_{cr,id}$ is derived from the Massonnet normal critical stress–shear critical stress domain [8] as follows:

$$\sigma_{cr,id} = \frac{\sqrt{\sigma_1^2 + 3\tau^2}}{\frac{1+\psi}{4}\cdot\frac{\sigma_1}{\sigma_{cr}} + \sqrt{\left(\frac{3-\psi}{4}\cdot\frac{\sigma_1}{\sigma_{cr}}\right)^2 + \left(\frac{\tau}{\tau_{cr}}\right)^2}} \tag{4}$$

where σ_1=130.9 MPa, τ=20.1 MPa are the design normal and shear stress values; $\sigma_{cr} = k_\sigma \cdot \sigma_{cr,0}$, $\tau_{cr} = k_\tau \cdot \sigma_{cr,0}$, being k_σ, k_τ the normal and shear stress buckling factors, and $\sigma_{cr,0}$ the elastic critical plate buckling stress of the equivalent orthotropic plate, expressed as $\sigma_{cr,0} = \frac{\pi^2 E}{12(1-\nu)}\left(\frac{t}{h}\right)^2$, with t=plate thickness and h=plate width (or mean width in case of variable section); and ψ is a coefficient that defines the linear variation of normal stress over the section, which can be set as equal to -1 in this case, by neglecting the very little contribution of the axial force to σ_1, quantified by a normal stress of 1.6 MPa. Panel 4 (Figure

5) results to be the most critical among the 13 web panels of type 1 beams. Considering its geometrical characteristics (base=b=1050 mm, h=2445 mm, t=5 mm), k_σ=27.6, k_τ=33 and $\sigma_{cr,0}$=0.78 MPa values come out, from which σ_{cr}=21.6 MPa and τ_{cr}=25.9 MPa are derived. By applying formula (4), $\sigma_{cr,id}$ results to be equal to 22.2 MPa.

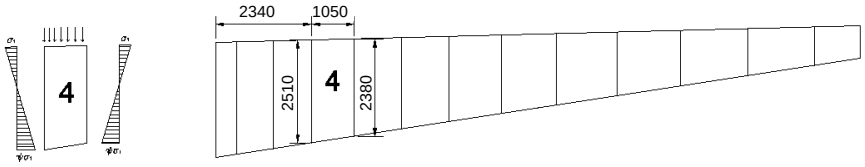

Figure 5: Geometry of panel 4 of type 1 beam (dimensions in millimeters)

The values of the normal and shear stress buckling factors are computed in [6] as a function of the aspect ratio α=b/h (whose average value is equal to 0.427 for panel 4) according to the expressions

$$k_\sigma = 15.87 + \frac{1.87}{\alpha^2} + 8.6\alpha^2 \quad \alpha < \frac{2}{3} \tag{5}$$

$$k_\tau = 4 + \frac{5.34}{\alpha^2} \quad \alpha < 1 \tag{6}$$

which provide good analytical approximations of the Timoshenko-Gere [9] original instability curves for linearly varying (with $\psi \leq 1$) normal stress, and uniform shear stress distributions, respectively. The difference between the $\sigma_{cr,id}$ and σ_{cr} values above is so little because of the great prevalence of σ_1 over τ, which produces a scarce influence of shear stress on the critical stress interaction domain. A second observation concerns σ_{cr}, which is greater than the value of 19.1 MPa derived by the Eurocode 3 – Part 1-5 [4] formula

$$\bar{\lambda}_p = \sqrt{\frac{f_y}{\sigma_{cr}}} = \frac{\bar{b}/t}{28.4\varepsilon\sqrt{k_\sigma}} \tag{7}$$

where $\bar{b}$ is the web width, $\varepsilon = \sqrt{\frac{235}{f_y}}$, and k_σ=23.9 for ψ=-1. The difference between the two σ_{cr} estimates is caused by the two k_σ values adopted (27.6 against 23.9). Indeed, unlike Standards [6], Eurocode 3 Part 1-5 [4] prudentially assumes the minimal theoretical value of 23.9—corresponding to α=2/3—for any aspect ratio of panels, when ψ=1.

2.3 Finite element buckling analysis

The finite element model of type 1 beams generated for the buckling analysis is constituted by a mesh of quadrilateral isoparametric shell elements with an average side of 150 mm. This dimension determines a number of constituting elements of each beam panel varying from around 80 to around 120, which is generally deemed appropriate for an accurate simulation of local buckling effects in laterally loaded stiffened or unstiffened plates [10-11]. Fixed end restraints are imposed to the end section of beams connected to the steel drum, whereas only

the lateral displacements are blocked on the tip end section, so as to reproduce exactly the restraint offered by the perimeter C-shaped edge beam of each mushroom roof panel.

The buckling analysis is developed in SAP2000NL by a classical eigenvalue formulation:

$$([K_E]+\lambda[K_G])\{v\}=\{0\} \tag{8}$$

where $[K_E]$ and $[K_G]$ are the elastic and geometric stiffness matrixes of the structural element or system, λ is the generic eigenvalue, and $\{v\}$ is the corresponding eigenvector. The solution of equation (8) provides the instability factors λ_i and the instability modal vectors $\{v_i\}$. The minimum among the λ_i multipliers computed by the program represents the first (or critical) eigenvalue λ_1. If λ_1 is greater than 1, no buckling occurs under the imposed loads.

The first mode buckling configuration of type 1 beams resulting from the analysis, displayed in Figure 6, highlights that the maximum lateral deformation is achieved in panel 4, consistently with the analytical assessment predictions.

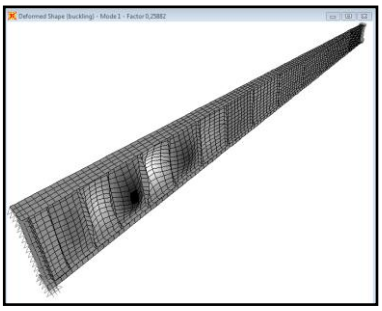

Figure 6: Deformed shape of type 1 beams obtained for the first buckling mode

The λ_1 factor is equal to 0.259. By multiplying this value by the maximum von Mises ideal stress obtained in the central zone of the panel for the first buckling mode deformed configuration, equal to 90 MPa, the following finite element critical ideal stress estimate $\sigma_{cr,id,FE}$ is deducted: $\sigma_{cr,id,FE}$=23.3 MPa. This value is very close to the $\sigma_{cr,id}$ normative estimate of 22.2 MPa given by formula (4), with a percent difference limited within 5%. Similar correlations are obtained for the subsequent local buckling modes too (the second mode achieves the maximum lateral displacements in panel 5, the third mode in panel 3, etc) as the differences between $\sigma_{cr,id}$ and $\sigma_{cr,id,FE}$ never exceed 5%.

The seventh and eighth buckling modes are the first two involving a global (lateral-torsional) instability deformed shape. The maximum lateral displacements and stresses are reached in the eighth mode, visualized in Figure 7 with an amplification factor of 5000. The horizontal projection is also plotted in this drawing, showing that the deformed shape corresponds, as for the seventh mode, to the first theoretical global buckling mode of the beams. The λ_8 eigenvalue is equal to 0.524, which must be compared to the unsafety factor $M_{b,Rd}/M_{Ed}$=0.586 resulting from the lateral/torsional buckling verification discussed in section 2.1. The difference between the two values is around 12%, and the numerical result in this case is more conservative than the normative factor estimate.

The data obtained from a computational analysis are always a function of the geometrical dimensions of the mesh. Mesh-sensitivity was investigated by varying the sides of the shell

elements by factors 2, 1.5, 0.75 and 0.5 with respect to the reference average dimensions of 150 mm.

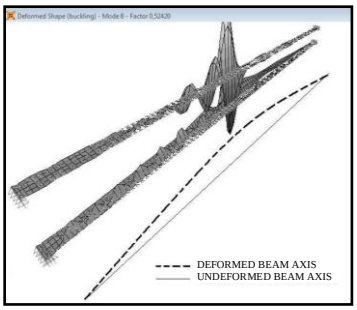

Figure 7: 5000-times magnified deformed shape of type 1 beams obtained for the eighth buckling mode

As a general result of this enquiry, no appreciable influence on eigenvalues and eigenvectors was observed when passing to the most refined meshes. A trend to a progressive increase of the eigenvalues emerges when increasing the sides (e.g., $\sigma_{cr,id,FE}$ in panel 4 becomes equal to 24.1 and 25.3 MPa for mesh factors 1.5 and 2, respectively), even if the shapes and the hierarchy of buckling modes are kept unchanged. Based on these observations, the average dimensions assumed for this analysis appear to be the maximum compatible with the accuracy of the solution, and thus they can represent a credible balance point between the need to reach accurate results and to constrain the computational effort. Limitedly to this case study, it can be concluded that the buckling analysis performed by SAP2000NL allows acceptably estimating the local and global critical buckling conditions of steel beams.

3 ANALYSIS OF R/C COLUMNS

A view of a monumental column during the construction phases of the building, and the sequence of geometrical sections along its height, are reproduced in Figure 8. As illustrated in these images, the shape of columns constantly varies from the base (cross-type section with 6 m-long and 1 m-wide sides) to the top (circular-type section, 2.5 m wide). The top section, reduced to a diameter of 2 m, is prolonged for further 1.6 m to form the groove where the triangular steel plates supporting the circular drum of the mushroom roof are positioned, as described in section 2.

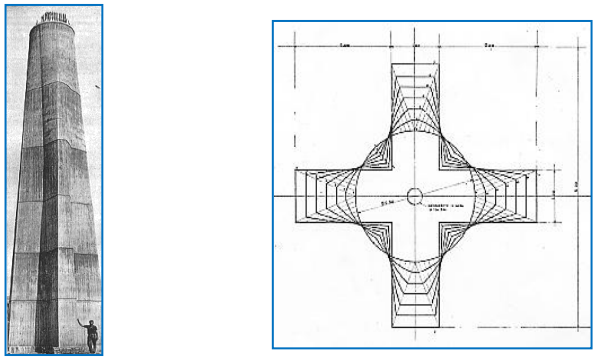

Figure 8: View of a column during the construction phases, and sequence of its geometrical sections

The drawings of the R/C sections at the base, at an intermediate height and on top, displayed in Figure 9, show an inner hole, where a spiral steel staircase to access the roof, and a conductor pipe are housed.

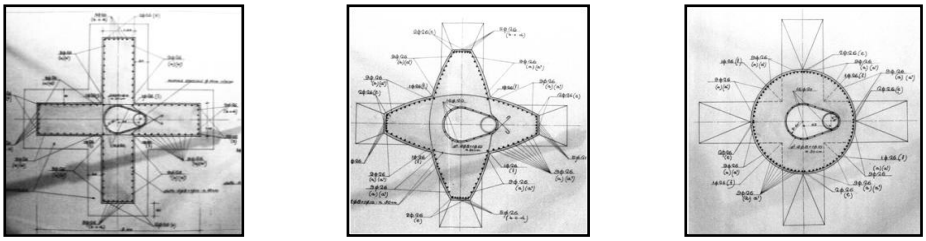

Figure 9: R/C sections at the base, an intermediate height and the top

As observed in the introductory section, an "integral" seismic pushover assessment analysis of the columns was carried out in view of their "uniform resistance" design conception. The model was generated with ANSYS [7] and is made of a full mesh of solid octahedral "concrete" elements, with embedded steel reinforcing bars that can be freely oriented with respect to the global coordinate system. A sketch of the geometry of a "concrete" element is shown in Figure 10.

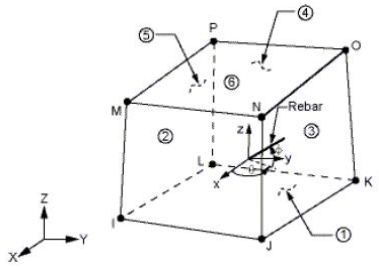

Figure 10: Geometrical representation of an octahedral "concrete" element with embedded reinforcing bars

The Willam-Warnke triaxial failure domain [12]—a three-dimensional view of which in the space of the principal stresses (σ_{xp}, σ_{yp}, σ_{zp}) normalized to the compressive strength f_c, and a projection of which on the σ_{xp}–σ_{yp} plane are displayed in Figure 11—is adopted to model the ultimate compressive, tensile and mixed compressive-tensile triaxial ultimate response of the concrete material. The classical Drucker-Prager yield criterion [13] is assumed by the program for plastic deformations. A bilinear strain-hardening elasto-plastic behaviour is assigned to reinforcing steel.

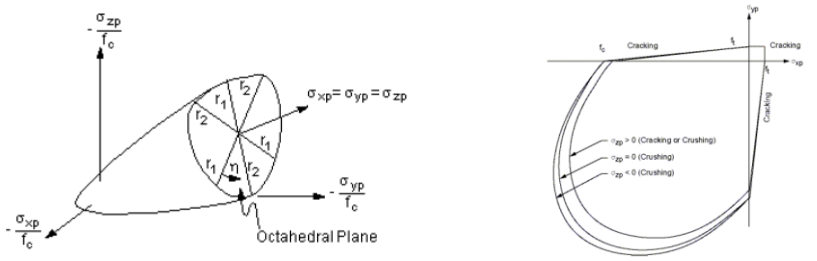

Figure 11: Representations of the Willam-Warnke failure domain

The main mechanical parameters of the "concrete" model are as follows: σ_o=shear transfer coefficient for an open crack, σ_c=shear transfer coefficient for a closed crack, f_t=uniaxial tensile cracking stress, f_c=uniaxial crushing stress, f_{cb}=biaxial crushing stress, E_c=Young modulus, and ν_c=Poisson ratio. The parameters of reinforcing steel are: f_y=yielding stress, s_h=kinematic strain hardening ratio, E_s=Young modulus, and ν_s=Poisson ratio. The parameters that define the surface of the Drucker-Prager domain are: c=cohesion, ϕ=friction angle, and ψ= dilatancy angle. The following values of these quantities were adopted in the analysis: σ_o=0.3, σ_c=0.85, f_t=1.7 MPa, f_c=23.8 MPa, f_{cb}=1.2 f_c, E_c=35600 MPa, ν_c=0.2; f_y=321.6 MPa, s_h=0.015, E_s=206000 MPa, ν_s=0.3, according to the characteristics of the materials; and c=2.12 MPa, ϕ=30º, ψ=0º (associated flow rule), from literature suggestions concerning the plasticity domain for concrete elements [7], [14-15].

The horizontal load for the development of the pushover process was applied to the top of the column. P-delta effects were taken into account, in view of the expected high maximum displacements. As for all types of incremental analysis, the critical parameter for the convergence and the accuracy of the numerical solution was represented by the number of sub-steps to be developed in the ramped loading process within any single load step, with the latter fixed at 10 mm. A displacement-based criterion for convergence control was adopted, with a tolerance of 5%. The following numbers of sub-steps were finally selected, after several tentative choices: 50 (corresponding to 0.2 mm) for steps 1 through 13, characterized by moderate cracking effects in the concrete elements; 200 (0.05 mm) for steps 14-27—extensive cracking in the tension zones; 300 (0.033 mm) for steps 28-70—softening response phase. These data confirm general suggestions [14] about the preferable values (ranging from 0.1 mm to 0.01 mm) of the displacement increments in full-cracking/crushing problems when the non-linear behaviour of a significant portion of the model is activated. Further increases of the number of sub-steps in the more accentuated non-linear response phases did not show any practical influence on the accuracy of the solution. Indeed, by amplifying the number of sub-steps by a factor up to 10, that is, by assuming up to 2000 sub-steps for steps 14-27, and up to 3000 sub-steps for steps 28-70, differences no greater than 0.1% on base shear were found.

For the assumed set of mechanical parameters, derived from the original design documentation of the building, the pushover analysis was concluded at the end of step 70, corresponding to a top displacement of 700 mm (drift ratio of 3.5%). At the current level of refinement of the model, this was assumed as the numerically determined structural collapse condition. The only two parameters not related to the specific characteristics of the constituting materials—σ_o and σ_c—were varied in their technical ranges of interest (σ_o from 0.2 to 0.4, σ_c from 0.65 to 0.9) to check their influence on response, which resulted to be negligible.

The base shear-top displacement capacity curve obtained from the analysis is plotted in Figure 12. A median vertical section reproducing the cracked configuration of the model at the end of the last step of the pushover analysis, and two views orthogonal to the loading direction showing the distributions of the vertical component of normal stress and the axial stress in reinforcing bars, are displayed in Figure 13. The following observations can be drawn from Figures 12 and 13.

- A remarkably smooth shape of the capacity curve emerges, as a consequence of the high number of sub-steps adopted in the analysis;

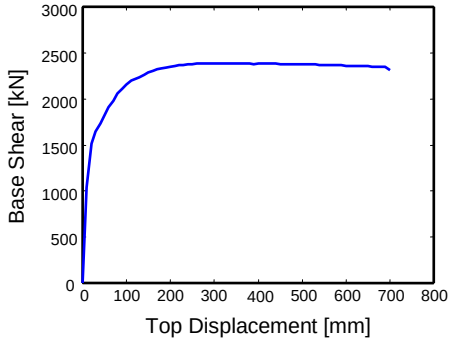

Figure 12: Response curve obtained from the pushover analysis

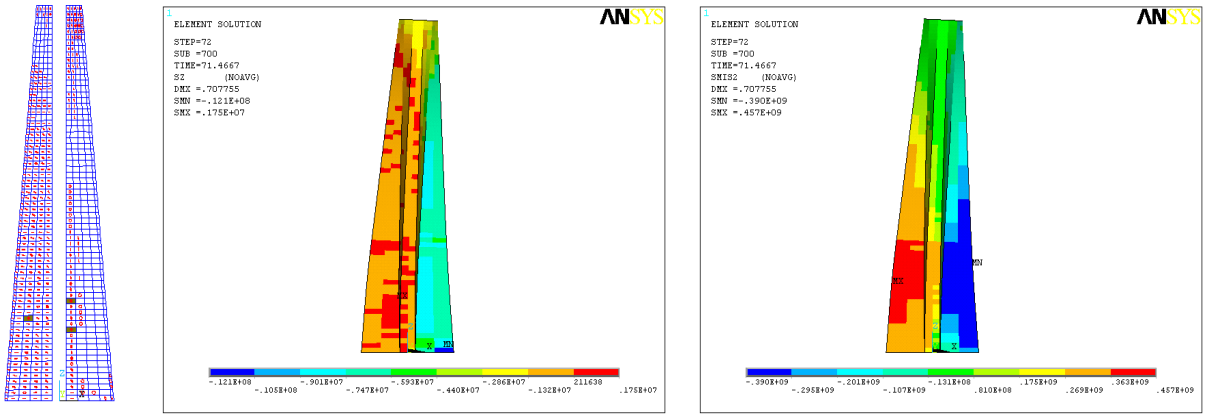

Figure 13: Cracked configuration of the model, vertical normal stress distribution, and stress distribution in reinforcing bars at the end of the last step of the pushover analysis

- The curve is rather linear up to around 1500 kN (with top displacement of 20 mm and drift ratio of 0.1%), that is up to around 60% the maximum base shear, equal to 2390 kN; then, cracking begins to develop significantly in the elements situated on the tension side, and the curve visibly gets non-linear elastic;
- This second response phase goes on up to a force of 2200 kN, with corresponding top displacement of 110 mm (drift ratio of 0.55%), when the first plasticization of reinforcing bars occurs;
- The plasticization then increases, determining nearly a plateau zone extended from around 250 mm to around 450 mm; the maximum shear force is reached for a displacement of 300 mm (drift ratio of 1.5%);
- A softening branch follows, featuring a strength degradation of around 0.2 kN/mm up to the last two steps, where the degradation reaches accentuated values of 0.5 kN/mm (step 69) and 2kN/mm (step 70), while it does not mean a sudden drop of strength in proximity to the numerical solution divergence point;
- Cracking extends rather uniformly over the tension side, whereas crushing is attained only in very few local elements situated around the inner hole (dark-coloured elements in the vertical section in Figure 13). This indicates that concrete is far from ultimate strength conditions on the compression side of the column at the last step of the analysis;

- This is confirmed by the distribution of the vertical components of normal stress, which shows maximum values no greater than 0.5 f_c, in the external fiber of base section;
- Plasticization of reinforcing bars is spread over 2/3 of the height of the column.

These observations highlight that numerical collapse is not determined by the failure of the constituting materials, but by the excessive deformation of the octahedral elements in various portions of the mesh. Deformation is not sensitive to the number of sub-steps, which was increased further to a value of 10000 in the 70th step to check its possible influence, without any practical consequences.

The response curve highlights acceptable behavioural capacities of columns, with no damage for rather high base shear values, and reasonably good ductility resources. A complete interpretation of the results of the pushover enquiry, based on a formal seismic assessment analysis, will be presented in forthcoming communications about this research.

ACKNOWLEDGMENTS

The study reported in this paper was financed by the Italian Ministry of Education, University and Research within the PRIN 2008 Project (Research Programme "Conceiving structures: engineering and architecture in Italy in the 1950s and 1960s. A multi-disciplinary research"). The authors gratefully acknowledge this financial support.

REFERENCES

[1] Sorace, S. and Terenzi, G. Structural and historical assessment of a modern heritage masterpiece: the "Palazzo del Lavoro" in Turin. Proc. STREMAH 2011, C. Brebbia and L. Binda, Eds., Chianciano Terme, Italy, WIT Press, Southampton (2011).

[2] Computers & Structures, Inc. *SAP2000NL, Structural Analysis Programs – Theoretical and users' manual*, Version No. 14.03, Berkeley, CA (2010).

[3] Eurocode 3. *Design of steel structures. Part 1-1: General rules and rules for buildings*. EN 1993-1-1, Bruxelles (2005).

[4] Eurocode 3. *Design of steel structures. Part 1-5: Design of plated structures*. EN 1993-1-5, Bruxelles (2006).

[5] NTC 2008. *New Technical Standards for constructions [in Italian]*. G.U., Rome, Italy (2008).

[6] CNR 10011. *Steel structures – Instructions for design, construction, testing and maintenance* [in Italian]. UNI, Milan, Italy (1997).

[7] Swanson Analysis System, Inc. *ANSYS, Engineering Analysis System – Theory/users' manual.* Release 10.0, Canonsburg, PA (2010).

[8] Massonnet, C. Rapport sur le theme II C: Poutres de grandes dimensions à âme mince. Proc. 8th AIPC Congress, New York, pp. 157-208 (1968).

[9] Timoshenko, S.P. and Gere, J.M. *Theory of elastic stability*. 2nd edition. Mc-Graw Hill, New York (1961).

[10] Mukhopadhay, M. and Mukherjee, A. Finite element buckling analysis of stiffened plates. *Computer & Structures* (1990) **34**:795-803.

[11] Chin, C.-K., Al-Bermani, F.G. and Kitipornchai S. Finite element for buckling analysis of plate structures, *Journal of Structural Engineering (ASCE)* (1993) **119**: 1048-1068.

[12] Willam, K.J. and Warnke, E.P. Constitutive model for the triaxial behaviour of concrete. Proc. IABSE Seminar on Concrete structures subjected to triaxial stresses, Bergamo, Italy, Vol. 19, pp. 1- 30 (1974).

[13] Drucker, D.C. and Prager, W. Soil mechanics and plastic analysis for limit design. *Quarterly of Applied Mathematics* (1952) **10**:157–165.

[14] Chen, W.F. *Plasticity in reinforced concrete*. Mc-Graw Hill, New York (1982).

[15] Borri, A., and Sorace, S. FE analysis strategies for structural materials with small tensile strength. *Journal of Pressure Vessel Technology (ASME)* (1993) **115**:156-163.